Nuclear spin-spin coupling in a van der Waals-bonded system: Xenon dimer

Juha Vaara, Matti Hanni, and Jukka Jokisaari

Citation: The Journal of Chemical Physics **138**, 104313 (2013); doi: 10.1063/1.4793745
View online: http://dx.doi.org/10.1063/1.4793745
View Table of Contents: http://scitation.aip.org/content/aip/journal/jcp/138/10?ver=pdfcov
Published by the AIP Publishing

Nuclear spin-spin coupling in a van der Waals-bonded system: Xenon dimer

Juha Vaara,[1,a)] Matti Hanni,[2] and Jukka Jokisaari[1]
[1]*NMR Research Group, Department of Physics, P.O. Box 3000, FIN-90014 University of Oulu, Finland*
[2]*Department of Chemistry, University of Munich, Butenandtstr. 7, D-81377 München, Germany*

(Received 8 January 2013; accepted 15 February 2013; published online 12 March 2013)

Nuclear spin-spin coupling over van der Waals bond has recently been observed via the frequency shift of solute protons in a solution containing optically hyperpolarized ^{129}Xe nuclei. We carry out a first-principles computational study of the prototypic van der Waals-bonded xenon dimer, where the spin-spin coupling between two magnetically non-equivalent isotopes, $J(^{129}\mathrm{Xe} - ^{131}\mathrm{Xe})$, is observable. We use relativistic theory at the four-component Dirac-Hartree-Fock and Dirac-density-functional theory levels using novel completeness-optimized Gaussian basis sets and choosing the functional based on a comparison with correlated *ab initio* methods at the nonrelativistic level. *J*-coupling curves are provided at different levels of theory as functions of the internuclear distance in the xenon dimer, demonstrating cross-coupling effects between relativity and electron correlation for this property. Calculations on small Xe clusters are used to estimate the importance of many-atom effects on $J(^{129}\mathrm{Xe} - ^{131}\mathrm{Xe})$. Possibilities of observing $J(^{129}\mathrm{Xe} - ^{131}\mathrm{Xe})$ in liquid xenon are critically examined, based on molecular dynamics simulation. A simplistic spherical model is set up for the xenon dimer confined in a cavity, such as in microporous materials. It is shown that the on the average shorter internuclear distance enforced by the confinement increases the magnitude of the coupling as compared to the bulk liquid case, rendering $J(^{129}\mathrm{Xe} - ^{131}\mathrm{Xe})$ in a cavity a feasible target for experimental investigation. © *2013 American Institute of Physics*. [http://dx.doi.org/10.1063/1.4793745]

I. INTRODUCTION

Indirect spin-spin coupling between magnetic nuclei *K* and *L*, *J*(*KL*), is mediated through the electron cloud of a molecule or solid.[1] Its use is in nuclear magnetic resonance (NMR) spectroscopy in investigating the electronic and atomic structure, due to its detailed dependence on the local surroundings of the two nuclei.[2] Spin-spin coupling between nuclei bonded over a covalent network has been known for decades and used, e.g., to reveal conformations of molecules through the well-known Karplus-type dependence of the isotropic three-bond spin-spin coupling constants on the dihedral angle.[3] Although spin-spin couplings over hydrogen bonds have been experimentally known for a considerably shorter time,[4] they, too, have found applications particularly in biomolecular science.[5]

Intermolecular spin-spin couplings over van der Waals bonds have been subjected to theoretical investigations using quantum-chemical electronic structure calculations. Bagno, Saielli, and Scorrano[6,7] reported *J*(CH) couplings in the range of 0.1–0.3 Hz in dimers of organic molecules at intermolecular distances favored by intermolecular potential. Both density-functional theory (DFT) and correlated *ab initio* approaches were used in these studies. The *J*(HH) coupling constant was found to be even smaller in such systems, and inclusion compounds were seen as the more likely candidate for experimental detection of such couplings. Earlier, Salsbury and Harris[8] used an elementary DFT method to arrive at the dependence of $J(^{129}\mathrm{Xe} - ^{131}\mathrm{Xe})$ in Xe_2 on the internuclear distance, obtaining small (in the millihertz range) and positive coupling constants for distances of relevance to the interacting Xe pair. Bagno and Saielli[9] used the relativistic zeroth-order regular approximation (ZORA[10]) DFT method and arrived at $J(^{129}\mathrm{Xe} - ^{1}\mathrm{H})$ and $J(^{129}\mathrm{Xe} - ^{13}\mathrm{C})$ below 1 Hz in complexes of Xe and organic compounds. $J(^{129}\mathrm{Xe} - ^{129}\mathrm{Xe})$ in Xe_2 as obtained by these authors indicated a sign change as a function of the internuclear distance. Their calculations were carried out at the scalar relativistic (neglecting spin-orbit effects), generalized gradient approximation level, with a doubly polarized triple-zeta (TZ2P) Slater basis set and frozen core. Pecul and co-workers investigated $J(^{3}\mathrm{He} - ^{3}\mathrm{He})$ in He_2 (Ref. 11) and $J(^{1}\mathrm{H} - ^{19}\mathrm{F})$ in the HF−CH_4 system,[12] with reasonably large values obtained at the equilibrium distance. These and related studies[13,14] imply that such through-space couplings require neither covalent nor hydrogen bond network joining the coupled nuclei. It furthermore appears that non-contact type interactions play a significant role in such couplings.

Experimental observation of spin-spin coupling over van der Waals bond was published in 2012 by Ledbetter *et al.*,[15] who performed solution-state measurements of the average coupling $\langle J(^{1}\mathrm{H} - ^{129}\mathrm{Xe})\rangle = -2.7 \pm 0.6$ Hz between the protons of pentane with hyperpolarized ^{129}Xe. The results were qualitatively verified by a combination of a molecular dynamics (MD) simulation and scalar relativistic quantum-chemical

a)Author to whom correspondence should be addressed. Electronic mail: juha.vaara@oulu.fi.

(DFT with ZORA) calculations,[15] which led to much larger couplings than predicted earlier.[8] The finding of coupling over van der Waals bonds opens new avenues for investigations of surface-physisorbed species as well as host-guest complexes featuring van der Waals interactions, particularly if the technique can be made nucleus-specific instead of average coupling involving several non-equivalent nuclei.

In this work we reconsider the prototypic van der Waals bonded system, the xenon dimer, and apply state-of-the-art four-component relativistic quantum-chemical methodology[16,17] to obtain predictions of $J(^{129}\mathrm{Xe} - {}^{131}\mathrm{Xe})$. Xenon isotopes are widely used as atomic guests, inert probes the NMR parameters of which are sensitive to the physical properties of the host material.[18] The sensitivity of Xe NMR can be greatly enhanced by spin exchange optical hyperpolarization techniques.[19] This particular choice of isotope combination is due to the fact that the spin-spin coupling between magnetically equivalent nuclei is not observable. As Xe is a heavy atom, relativistic quantum-chemical methods are mandatory for a reliable calculation of its spin-spin couplings. This is already apparent from the multiplicative *a posteriori*, hydrogen-like relativistic correction factor of the atomic magnetic hyperfine interaction (1.4242 for the Xe 5*s* shell, to be used to multiply the nonrelativistic Fermi contact interaction), as tabulated in Ref. 20. In addition to the approximate ZORA methodology mentioned above,[9,10,15] DFT-based, fully relativistic four-component methods are now available for *J*-coupling in the DIRAC software.[16] However, the presently used DFT functionals have not been found very reliable for the NMR properties of xenon[21–24] or intermolecular couplings,[13] mainly due to deficiencies appearing already at the nonrelativistic (NR) level as calibrated by highly correlated *ab initio* calculations. Therefore, we investigate also hybrid levels of theory in which such correlated NR calculations (currently unavailable at the relativistic level) are combined with relativistic effects obtained as differences between fully relativistic and NR calculations at the DFT and uncorrelated Hartree-Fock levels.

Besides the early reports of *J*(XeXe)-coupling in Refs. 8 and 9, the NMR properties of Xe_2 have been studied using quantum-chemical techniques with varying means of accounting for the relativistic effects.[9,21,22,25–28] In Ref. 29 it was noted that the nuclear shielding constants of Xe in Xe_n clusters can be modeled to a good accuracy as a superposition of pairwise interactions with neighboring Xe atoms at various distances. This would imply that also $J(^{129}\mathrm{Xe} - {}^{131}\mathrm{Xe})$ as an explicit pair interaction property is relatively independent of the presence of third bodies, and we show by quantum-chemical calculations of the Xe_3 and Xe_4 clusters that this indeed holds to a fair extent. This, in turn, paves the way to a simple estimate of the average $\langle J(^{129}\mathrm{Xe} - {}^{131}\mathrm{Xe})\rangle$ in samples of liquid xenon via MD simulation, as well as estimating the property for Xe_2 confined to a material cavity, such as in fullerenes or molecular sieves. In these studies we make explicit use of the accurate *ab initio* pair potential for Xe_2 obtained in Ref. 21. To model confined Xe_2, we construct a simplistic spherical cavity model, where the Xe atoms experience an interaction with the cavity walls described by an empirical Fermi function.

II. MODELLING

A. Quantum-chemical calculations

We carried out fully relativistic, four-component Dirac-Hartree-Fock (DHF) and Dirac-DFT electronic structure calculations of $J(^{129}\mathrm{Xe} - {}^{131}\mathrm{Xe})$ using the DIRAC software at different internuclear separations. NR calculations at HF, DFT, and the *ab initio* second-order polarization propagator with coupled-cluster singles and doubles amplitudes [SOPPA(CCSD)[30]] methods were performed using the DALTON[31] package.

1. Basis set

We used the primitive 27*s*25*p*21*d*1*f* basis originally developed for the magnetic properties (hyperfine coupling and electronic *g*-tensor) of ^{129}Xe in a van der Waals complex with the rubidium atom.[32] This basis has been obtained using the completeness-optimization paradigm,[33] where the parameters of basis functions as well as their number are determined to produce, for all the involved angular momentum values, a flat completeness profile[34] over a Gaussian exponent range wide enough to saturate the computational results for the studied physical properties, with as few functions as possible to a given accuracy criterion. This method of obtaining basis sets does not involve atom-specific calculations and is, hence, universal to those atoms and properties for which the found exponent range is sufficient. Completeness-optimized primitive basis sets have been used to obtain results close to the basis-set limit for magnetic[32,33,35–37] and magneto-optic properties,[38,39] as well as electron momentum densities.[40] In particular, Refs. 36, 37, and 39 have extended the application of the method to elements beyond the first row, xenon in two of the cases. The exponents of the present basis set are given in Table 1 of the supplementary material.[41] The basis is well-suited for the problem of $J(^{129}\mathrm{Xe} - {}^{131}\mathrm{Xe})$ in Xe_2, as also the original application[32] involves both a van der Waals bond and similar quantum-mechanical operators as the ones involved for the property at hand. Attempts were made to extend the basis by further diffuse *spdf* functions centered at the atoms or "ghost" functions situated mid-way between the nuclei. These measures led to insignificant changes of $J(^{129}\mathrm{Xe} - {}^{131}\mathrm{Xe})$, of ca. 1% of the coupling constant of −18.87 Hz obtained at the DHF level at the equilibrium internuclear distance $r_e(\mathrm{XeXe}) = 4.363$ Å of the dimer.[42] Hence, such additions were abandoned. The fact that accurate interaction-energy calculations[21] do require mid-bond functions underlines the greater sensitivity of particularly the electron correlation energy to the basis set, than in the case of NMR properties that are dominated by one-electron operators emphasizing the atomic core region.

The exponents of the 27*s*25*p*21*d*1*f* basis were employed in both the NR calculations and in the large-component wave function of the four-component calculations. In the latter, we used the unrestricted kinetic balance (UKB) prescription to obtain the small-component basis. Enhanced basis-set convergence for magnetic properties has been reported by this method as compared to the restricted kinetic balance method

that leads to a more compact small-component basis.[22,43–45] Similar improvements have recently been reported by the economic simple magnetic balance approach.[46]

2. Numerical aspects

A calibration study was carried out at r_e, where we found out that it is entirely safe to approximate the two-electron integrals involving only the small-component basis functions [the (SS|SS)-integrals] by the classical repulsion of tabulated atomic small-component charges.[47] Indeed, the change involved in this approximation was only 0.01 Hz at the DHF level at r_e. The convergence criterion of 1.0×10^{-7} in the linear response calculation[16] and the default numerical integration grid (in DFT calculations) of the DIRAC code were found sufficient at r_e. However, a slight improvement of the numerical fits (*vide infra*) of $J(^{129}\mathrm{Xe} - {}^{131}\mathrm{Xe})$ to a function describing the internuclear distance dependence of this property, was obtained at the DFT level after adopting the 1.0×10^{-8} convergence threshold and "ULTRAFINE" integrals. Therefore, these choices were used in the DFT (B3LYP) *J*-coupling curve. In the NR DFT calculations by the DALTON program, the "ULTRAFINE" integration grid[31] was further tightened in its radial part to the parameter value of 1.0×10^{-16} in single-point calculations at r_e, and further to 1.0×10^{-17} in calculations of the *J*-coupling curve. In DIRAC, we used the default non-collinear[48] definition of spin density.

3. Quantum-chemical models

At r_e we performed *ab initio* HF and SOPPA(CCSD) calculations (the latter method only at the NR level), as well as used DFT with BLYP,[49,50] B3LYP,[51] and BHandHLYP[52] exchange correlation functionals. These functionals cover the values of the exact exchange admixture parameter (EEX) of 0%, 20%, and 50%. Upon repeated calibration studies of hyperfine parameters (Refs. 23, 38, 39, 45, and 53, and references therein), particularly of xenon, EEX has been found to be the single most important parameter controlling the accuracy of DFT calculations as referenced against correlated *ab initio* calculations. Whereas no universally applicable value of EEX can be selected as the other parameters of the functionals also influence, quite often the best agreement with coupled-cluster level results is obtained by hybrid functionals with EEX in the neighborhood of 20%–50%. A point to note concerning calculations involving heavy elements, such as Xe, is that such calibrations need to be performed at the NR level, as methods for second-order magnetic property calculations have not yet been developed at relativistic correlated *ab initio* levels. In a similar vein, we do not yet have experimental data for $J(^{129}\mathrm{Xe} - {}^{131}\mathrm{Xe})$ over a van der Waals bond at our disposal, and selection of the relativistic DFT method using more accurate calculations at the (as such physically well-defined) NR level is the best that can be done presently. In this sense, we have taken a quite empirical approach in our DFT calculations.

We carried out a basic study at the Dirac-B3LYP (DB3LYP) level of the many-atom effects on $J(^{129}\mathrm{Xe} - {}^{131}\mathrm{Xe})$ by calculating the property for a Xe_3 cluster, with the atoms forming an equilateral triangle with r_e side length, as well as for Xe_4, where the atoms are arranged at the vertices of a tetrahedron, at internuclear distances equal to r_e. The findings were compared to those for geometry-optimized Xe_n ($n = 2, 3, 4$) clusters.

4. Internuclear distance dependence

To obtain the spin-spin coupling curves $J(r)$ we carried out calculations at 35 internuclear distances r from $r = 3$ Å to $r = 6$ Å in steps of 0.1 Å, with additional points at r_e, 6.2 Å, 6.5 Å, and 7 Å. For the purposes of analytical integrations and analyzing the MD trajectory (*vide infra*), we fitted the quantum-chemical data to the analytical form

$$J(r) = A/r^{p_0+p_1 r+p_2 r^2}, \tag{1}$$

where A and the p_i are adjustable parameters. As before,[21,22,25,28,29] we imply no physical interpretation of this form, but regard this merely as a convenient way of representing the data. We performed least-squares fits using a weighted procedure, where the modified Boltzmann factors $r^2 \exp[-V(r)/kT]$ appropriate for the best *ab initio* interatomic potential energy function of Ref. 21, $V(r)$, was used. The temperature T used in the fits was selected to (somewhat arbitrarily) correspond to liquid xenon at ambient pressure, 163 K. The factor r^2 in the weight function comes from the volume element of spherical polar coordinates. The purpose of the weighting procedure was to emphasize the data appropriate to the internuclear distance range at which the pairs of Xe atoms are typically found. Whereas very high-quality fits were obtained for *ab initio data* [HF, DHF, and SOPPA(CCSD)], the quality of the fits is clearly inferior (RMS deviation 100-fold) at the DFT levels, presumably due to residual noise in the quantum-chemical data originating in the best available numerical integration grids in DALTON and DIRAC.

B. Simulations of liquid xenon

MD simulation of a sample of $N = 2000$ Xe atoms was performed on the GROMACS[54] software and the *ab initio* interatomic potential energy function obtained in Ref. 21, using a recipe similar to that of Ref. 28. The simulations were performed under periodic boundary conditions in a cube-shaped simulation box with the side length equal to 52.2771 Å. The used interaction potential is based on calculations at the CCSD(T) level using scalar-relativistic pseudopotentials, bond basis functions, and core-polarization contributions, and its r_e and well depth are in good agreement with the empirical Aziz-Slaman potential.[42] The chosen state point corresponds to the pressure of $p = 5.2$ atm, the experimental number density of $n = 521.03$ amg, and temperature $T = 180$ K appropriate to liquid xenon, as depicted in the phase diagram in Ref. 55. The production runs were performed in the NVE ensemble using the velocity-Verlet algorithm with the integration time step of 1 fs. The final NVE simulation was started from the previous MD simulation of Ref. 28, and was first equilibrated for 300 ps, after which the production trajectory was accumulated for ca. 1 ns. The

snapshots of the production phase of the simulation were saved to disk at each 1000th time step. The Xe–Xe radial distribution function $g(r)$ was calculated from snapshots obtained at each 10th time step.

The lifetime of the instantaneous Xe_2 species occurring in the liquid was obtained by calculating the autocorrelation function (ACF)

$$C(\Delta t) = \sum_i \langle s_i(0); s_i(\Delta t)\rangle / \langle s_i^2 \rangle \qquad (2)$$

and fitting it to the monoexponential decay $f(\Delta t) = A \exp(-\Delta t/\tau)$, with Δt in the range of 10–50 ps. Here, $s_i(t)$ equals 1/0 to indicate the existence/non-existence of the dimer i,[56] according to whether or not the Xe–Xe distance is below 5.5 Å. The ACF was calculated from roughly 500 000 Xe pairs in a total length of ca. 65 ps.

C. Cavity model

To investigate $J(^{129}\text{Xe} - {}^{131}\text{Xe})$ for Xe_2 confined in cavities of porous materials, we constructed a spherically symmetric model cavity illustrated in Figure 1. In the model, the movement of the Xe atoms is limited by a Xe-wall potential of the form of the Fermi function

$$V_{\text{cav}}(R_i) = \frac{V_\infty}{1 + \exp[-(R_i - R_{\text{cav}})/w]}, \qquad (3)$$

where R_i is the distance of the ith Xe atom from the center of the cavity, R_{cav} is the cavity radius, V_∞ the depth of the confinement potential well, and w a parameter controlling the steepness of the wall. This functional form is characterized by a flat region in the potential profile at the center of the well, meaning that the confined Xe dimer does not experience forces when both its atoms reside in the interior of the cavity. The Xe atoms interact with each other with the same potential $V(r)$ that was used for the MD simulation (*vide supra*). In our model, the locations of the two Xe atoms are $\mathbf{R}_i = \mathbf{R}_c \pm \mathbf{r}/2$, with $\mathbf{R_c} = (R_c, \theta_c, \phi_c)$ (in spherical polar coordinates) specifying the location of the mid-point of the internuclear vector, $\mathbf{r} = (r, \theta, \phi)$. The total potential energy of the system is, hence,

$$V_{\text{tot}}(r, R_1, R_2) = V(r) + V_{\text{cav}}(R_1) + V_{\text{cav}}(R_2) \qquad (4)$$

and the thermally averaged spin-spin coupling of the dimer can be obtained by 6-dimensional numerical integration from

$$\langle J \rangle = \frac{\int d\mathbf{r} \int d\mathbf{R}_c \, J(r) \exp[-V_{\text{tot}}(r, R_1, R_2)/kT]}{\int d\mathbf{r} \int d\mathbf{R}_c \exp[-V_{\text{tot}}(r, R_1, R_2)/kT]}. \qquad (5)$$

The integration was performed on the MATHEMATICA code[57] at three temperatures: 150, 300, and 450 K. In the present context, the application of classical statistical mechanics in Eq. (5) involves a negligible error for the relatively heavy Xe atoms. The parameters ($w = 0.3$ Å and $V_\infty/k = 3500$ K) of the wall potential, Eq. (3), were selected empirically such that the $\langle J \rangle$ results were not sensitive to variations of the parameters around the chosen values. The value of V_∞ can be related to the depth of the Xe-Xe potential well,[21] 283.1 K.

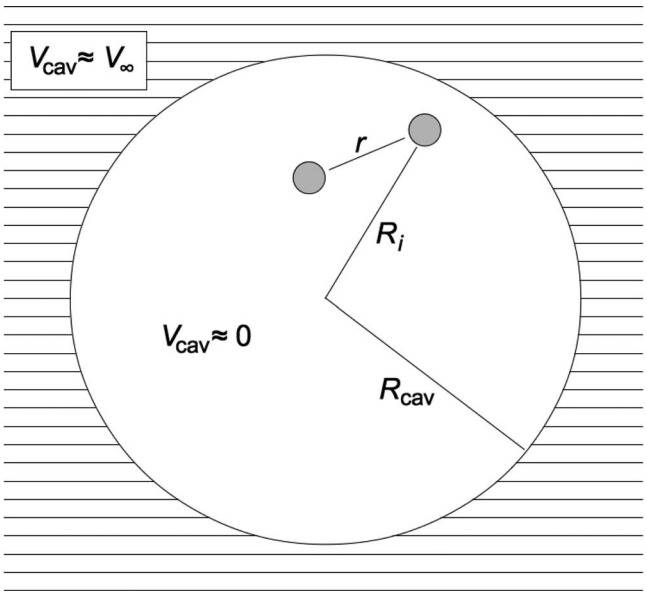

FIG. 1. Spherical cavity model for investigations of XeXe spin-spin coupling in confined Xe_2.

III. RESULTS AND DISCUSSION

A. Xe dimer at the equilibrium distance

Table I summarizes the quantum-chemical results for $J(^{129}\text{Xe} - {}^{131}\text{Xe})$ at the equilibrium internuclear distance according to the Aziz-Slaman potential. A point to note about Hartree-Fock spin-spin coupling calculations is that this level of theory is well-defined for systems such as the present one, which are not susceptible to triplet instability.[59] In general, the restricted Hartree-Fock method should be avoided for properties that involve electron spin-dependent perturbations. Furthermore, in calculations with varying internuclear distance, the presently used single-reference methods have no particular problems, as the ground state of Xe_2 remains well-described by a single electronic configuration at all values of r.

Our primary point of reference for the quality of the results is the NR SOPPA(CCSD) level of theory. We repeat that there are neither experimental results for Xe_2 to calibrate our data with, nor correlated *ab initio* methods at the relativistic level. At both the NR and relativistic levels, the results of Table I progress systematically towards more negative values as functions of EEX in the functionals, noting that the HF method corresponds to EEX = 100%. The nonrelativistic SOPPA(CCSD) datum is located in between the B3LYP and BHandHLYP values, relatively close to the former, as often found for hyperfine properties. As B3LYP provides also the closest agreement with the detailed physical contributions to J at the NR level, broken down in Table I, we choose B3LYP as the primary functional by which we carry out further DFT studies both at the NR and relativistic levels. Reference 13 reported a comparison of CCSD and B3LYP results for intermolecular couplings, with the latter level consistently providing the correct sign and order of magnitude. The present relative magnitudes of the different NR contributions resemble the findings of Bagno and Saielli[9] and Pecul *et al.*[12] in that, besides the dominating contact term, also the

TABLE I. Calculated spin-spin coupling constant $J(^{129}\mathrm{Xe} - {}^{131}\mathrm{Xe})$ (in Hz) in xenon dimer at the equilibrium internuclear distance (4.363 Å) at nonrelativistic (NR) and 4-component relativistic (Rel.) levels, as well as the different physical contributions at the NR level.[a]

	Total coupling constant		Physical contributions to NR result[b]			
Method	NR	Rel.	DSO	PSO	SD	FC
Hartree-Fock	− 13.81	− 18.87	0.00	3.33	− 0.45	− 16.69
SOPPA(CCSD)	− 9.91	. . .[c]	0.00	3.64	− 0.49	− 13.06
BHandHLYP	− 11.99	− 16.44	0.00	4.05	− 0.50	− 15.54
B3LYP	− 8.11	− 11.22	0.00	4.64	− 0.48	− 12.27
BLYP	− 6.07	− 8.58	0.00	5.22	− 0.46	− 10.83

[a]Calculations at the indicated level of theory using the basis set of Table I of the supplementary material.[41]
[b]Contributions of the dia- and paramagnetic nuclear spin-electron orbit (DSO and PSO, respectively), spin-dipole (SD), and Fermi contact (FC) contributions[58] to J at the NR level.
[c]Correlated *ab initio* levels of theory are not available for relativistic calculations of J.

orbital contribution (PSO) is of importance, and the spin-dipole term is unimportant.

Relativistic effects are seen to increase the absolute value of the coupling constant by a factor of ca. 1.4, regardless of the level of theory used. It is noteworthy that this factor is distinctly smaller than what would be expected from the above-mentioned hydrogen-like scaling parameter,[20] $1.4242^2 \approx 2$, indicating that, while such *a posteriori* correction factors can be used to assess the order of magnitude of the relativistic influences, they are not quantitative. Correlation effects, calculated as the difference of the electron-correlated result from the Hartree-Fock datum at either the NR or relativistic level, diminish the absolute value of the coupling constant. The relative magnitudes of correlation effects range from more than 50% to 13% at DFT levels from BLYP to BHandHLYP, respectively. The fact that the overall results for J are larger at the relativistic level than nonrelativistically, means then that the correlation effects at the relativistic level are larger in the absolute sense. The data indicate, therefore, coupling between relativistic and correlation effects.

B. Many-atom effects

Table II illustrates the importance of many-atom effects on $J(^{129}\mathrm{Xe} - {}^{131}\mathrm{Xe})$, based on calculations of Xe_3 and Xe_4. The results indicate a decreasing trend of the absolute value of the spin-spin coupling, which is a pair property, upon adding Xe atoms to the cluster. The changes amount to less than 1 Hz per additional atom, in these systems where all the atoms are in close contact with each other. Geometry optimization of the clusters leads to somewhat smaller many-atom effects than using interatomic distances equal to r_e. The order of magnitude of the results remains, however, for the different clusters regardless of whether they are geometry-optimized or not, which qualitatively confirms that a pairwise additive model may be meaningfully used to analyze the J coupling in condensed phases, such as in the liquid Xe simulations discussed below.

Reference 29 investigated the pairwise additivity of the nuclear shielding interactions in Xe clusters, sampling systems up to Xe_{12} featuring a range of internuclear distances and Xe coordination numbers, Z. While a pairwise additive model was able to account for many-body situations with a low Z, for an accurate treatment of condensed-phase conditions with Z up to 11 it was necessary to employ an effective binary property curve, with the many-atom effects implicitly included in its fitting parameters. Table II also includes scaled chemical shift data for the three smallest clusters studied in Ref. 29, divided by Z in each case to make them comparable to the pair interaction property J(XeXe). We note that the pair interaction effect on the xenon shift also experiences a practically constant (about 2 ppm) decrease upon successive addition of Xe atoms, qualitatively in a manner similar to the present data for J. Considering the different character of the two properties (δ and J) and the different theoretical methods used in their calculation in Ref. 29 and here, respectively, this interesting similarity calls for further investigations of many-atom effects on J couplings.

C. Spin-spin coupling curves

The calculated and fitted [Eq. (1)] data for $J(^{129}\mathrm{Xe} - {}^{131}\mathrm{Xe})$ as functions of internuclear distance are illustrated in Figs. 2(a) and 2(b), whereas the other panels of the same figure focus on the comparison of [Fig. 2(c)] relativistic and

TABLE II. Calculated spin-spin coupling constant $J(^{129}\mathrm{Xe} - {}^{131}\mathrm{Xe})$ in small xenon clusters. For comparison, calculated data from Ref. 29 for the Xe chemical shift δ in the same clusters are shown, divided by the number of neighbor atoms (coordination number Z), in each case. The internuclear distances are equal to 4.363 Å, the r_e distance appropriate to the Aziz-Slaman interatomic potential, unless otherwise noted.

System	J (Hz)[a]	J (Hz)[b]	Z	δ/Z (ppm)[c]
Xe_2	− 11.22	− 9.65	1	29.02
Xe_3	− 10.51	− 9.11	2	26.80
Xe_4	− 9.65	− 8.42	3	24.65

[a]Relativistic DB3LYP calculations using the basis set of Table I of the supplementary material.[41]
[b]As footnote (a) but at cluster geometries optimized at the CCSD(T) level with relativistic effective core potentials and modified cc-pVQZ valence basis sets, as detailed in Ref. 21. The optimized bond lengths for the different clusters are, in Å: 4.4316 (Xe_2), 4.4318 (Xe_3), and 4.4300 (Xe_4).
[c]Reference 29. Chemical shifts obtained from calculated Xe shielding constants σ as $\delta = \sigma(\text{free Xe}) - \sigma(Xe_n)$, divided by the number of nearest neighbors Z. Nonrelativistic Hartree-Fock calculations.

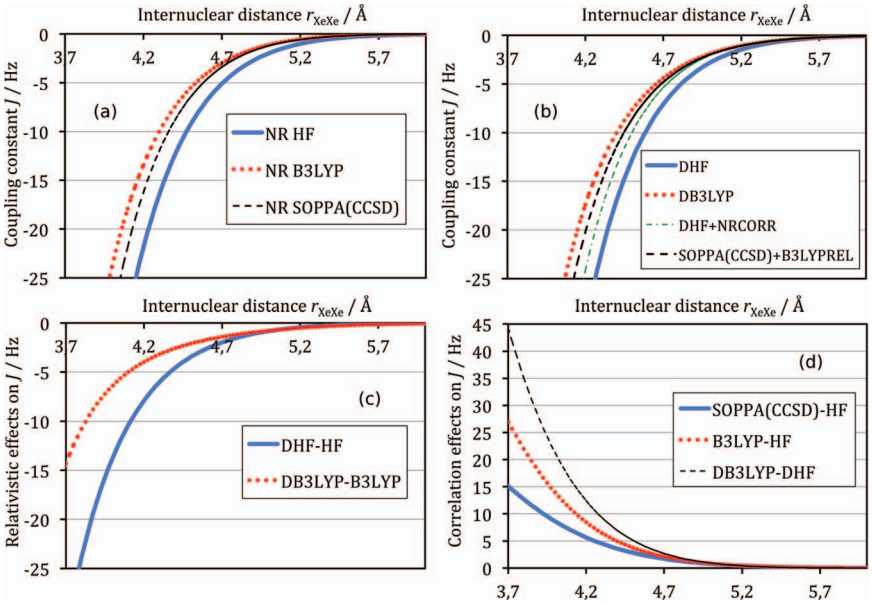

FIG. 2. Calculated internuclear distance dependence of the spin-spin coupling constant $J(^{129}\mathrm{Xe} - {}^{131}\mathrm{Xe})$ in xenon dimer. (a) Nonrelativistic (NR) calculations at the Hartree-Fock (HF), B3LYP (DFT), and *ab initio* SOPPA(CCSD) levels of theory. (b) Relativistic calculations at the Dirac-Hartree-Fock (DHF) and Dirac-B3LYP (DB3LYP) levels, as well as at the following hybrid levels of theory: DHF combined with the electron correlation effects estimated at the NR level of theory according to Eq. (6) (DHF+NRCORR) and NR SOPPA(CCSD) combined with relativistic effects estimated at the B3LYP level of theory according to Eq. (7) [SOPPA(CCSD)+B3LYPREL]. (c) Comparison of relativistic effects at the non-correlated (DHF-HF) and DFT (DB3LYP-B3LYP) levels of theory. (d) Comparison of electron correlation effects at the NR [SOPPA(CCSD)-HF and B3LYP-HF] as well as at the relativistic levels of theory (DB3LYP-DHF). The curves are fits to Eq. (1).

[Fig. 2(d)] electron correlation effects at various levels of theory. The original quantum-chemical data and the fitting parameters of the functional form of Eq. (1) are listed in the supplementary material.[41]

The J-coupling curves further underline the findings at r_e: relativistic effects increase and electron correlation effects decrease the absolute value of the coupling constant. As judged by a comparison of the SOPPA(CCSD) and B3LYP results at the NR level, electron correlation effects are somewhat exaggerated by B3LYP. In order to arrive at as realistic as possible predictions for the interatomic coupling curves, we also constructed two distinct hybrid levels of theory. In the first, relativistic effects at the uncorrelated level (DHF) are combined with the correlation effects obtained nonrelativistically as

$$J(\mathrm{Rel.}+\mathrm{Corr.}) = J(\mathrm{DHF}) + \{J[\mathrm{SOPPA(CCSD)}] - J(\mathrm{HF})\}. \quad (6)$$

In the second method we adopted the opposite approach, and combined the NR SOPPA(CCSD) data with relativistic effects obtained at the B3LYP level,

$$J(\mathrm{Corr.}+\mathrm{Rel.}) = J[\mathrm{SOPPA(CCSD)}] + \{J(\mathrm{DB3LYP}) - J(\mathrm{B3LYP})\}. \quad (7)$$

It can be seen in Fig. 2(b) that these levels, which combine relativistic and electron correlation effects in two different ways, fall in between the "pure" relativistic DHF and DB3LYP curves. Figures 2(c) and 2(d) indicate significant cross-coupling effects in the correlation and relativistic effects for this property. Among the two hybrid methods, only the latter, Eq. (7) is capable of accounting for these effects. Therefore, it constitutes the most reliable approximation that we have at our disposal presently. At r_e, these hybrid parametrizations correspond to values of the coupling constant $J(^{129}\mathrm{Xe} - {}^{131}\mathrm{Xe})$ equal to (in Hz) −14.98 ("Rel.+Corr" parametrization) and −12.71 ("Corr.+Rel."). As noted above, the ratio of relativistic and nonrelativistic results is to a good accuracy a constant number at the various levels of theory and at a relatively broad range of internuclear distances around r_e. Scaling the NR SOPPA(CCSD) result at r_e by the ratio $\mathrm{DHF}(r_e)/\mathrm{HF}(r_e) \approx 1.37$, we end up at an estimate of what a relativistic SOPPA(CCSD) result could be, if the methodology for such calculations existed. The result obtained by this procedure is −13.55 Hz, in between the "Corr.+Rel." and "Rel.+Corr." parametrizations, relatively close to the former. Were the homonuclear coupling $J(^{129}\mathrm{Xe} - {}^{129}\mathrm{Xe})$ experimentally observable, an estimate of its magnitude at r_e would be obtained from the "Corr.+Rel." parametrization by

$$J(^{129}\mathrm{Xe} - {}^{129}\mathrm{Xe}) = \frac{\gamma(^{129}\mathrm{Xe})}{\gamma(^{131}\mathrm{Xe})}\, J(^{129}\mathrm{Xe} - {}^{131}\mathrm{Xe}) = 42.88\ \mathrm{Hz}, \quad (8)$$

using the gyromagnetic ratios γ of the two isotopes.

D. Spin-spin coupling in liquid xenon

Average of a pair interaction property, such as $J(r)$, can be obtained by analyzing the individual Xe–Xe pairs that occur in a simulation, as

$$\langle J \rangle = \frac{1}{N(N-1)/2} \sum_{i=1}^{N-1} \sum_{j=i+1}^{N} J(r_{ij}). \quad (9)$$

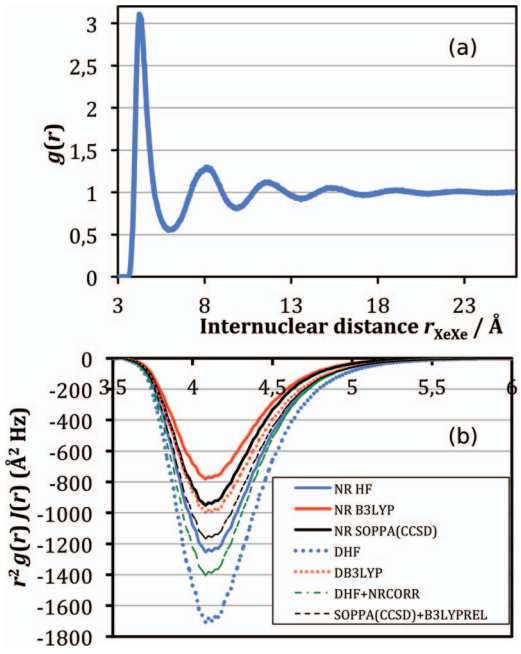

FIG. 3. (a) Simulated radial distribution function in liquid Xe. (b) The integrand of Eq. (10) on the basis of the simulated $g(r)$ and the spin-spin coupling curves $J(r)$ obtained at various theoretical levels (see Fig. 2 for the abbreviations).

The same quantity can be obtained also through the simulated radial distribution function $g(r)$ as[60]

$$\langle J \rangle = \lim_{r_{\max}\to\infty} \frac{4\pi}{V_{\rm sp}(r_{\max})} \int_0^{r_{\max}} r^2 g(r) J(r)\, dr, \qquad (10)$$

where $V_{\rm sp}(r_{\max})$ is the volume of a sphere of radius $r_{\max}$. For a simulation in a cube-formed box of side length L, $r_{\max}$ equals $L/2$. The presently simulated $g(r)$ of liquid Xe is depicted in Fig. 3, together with the integrand $r^2 g(r) J(r)$ of Eq. (10).

The two methods for obtaining $\langle J \rangle$ in our simulation sample according to Eqs. (9) and (10) are consistent, as both give the following results (in mHz) at the indicated theoretical levels used for parametrizing $J(r)$: −128.9 (NR HF), −79.3 (NR B3LYP), −95.1 [NR SOPPA(CCSD)], −176.5 (DHF), −105.1 (DB3LYP), −142.6 [Eq. (6)], and −120.9 [Eq. (7)]. A very good quality of statistical sampling is indicated by the maximum difference observed for the two methods equalling 0.02 Hz, as well as the statistical standard errors of mean that are the order of 0.01 Hz. These errors are entirely insignificant as compared to the—in this scale, large—deficiencies in the theoretical model, primarily the neglect of many-atom effects and the approximations in the quantum-mechanical calculations.

The above simulation results cannot, however, be related to the value of $J(^{129}\mathrm{Xe} - {}^{131}\mathrm{Xe})$ in bulk liquid xenon, as they are obtained with the rather arbitrary choice made for the simulation cell size. In fact, for an infinitely large simulation cell, represented in Eq. (10) by $r_{\max} \to \infty$, the average coupling constant decays to zero as the inverse of the number of atoms N. This can be seen from Eq. (9), where the denominator scales as $\mathcal{O}(N^2)$ whereas the numerator increases only linearly with N due to the finite spatial extent of the function $J(r)$. Figure 3(b) reveals that contributions to the average coupling are only obtained from Xe–Xe pairs that have the internuclear separation within the range 3.5–5.5 Å.

In traditional NMR techniques, whether a spectral feature can be resolved or not is determined by the relation of the rate of the dynamical process(es) related to the feature, to its NMR time scale.[61] For $\langle J(^{129}\mathrm{Xe} - {}^{131}\mathrm{Xe})\rangle$, the relevant dynamical process is the exchange of ^{131}Xe atoms into and out from the first solvation shell of an ^{129}Xe atom (or *vice versa*). The lifetime of sc. "permanent" Xe dimers in Xe gas at 1 amg number density and 295 K temperature has been evaluated to be 200 ± 60 ps in the simulations of Ref. 28. With the value of $|J(^{129}\mathrm{Xe} - {}^{131}\mathrm{Xe})|$ at the r_e separation being ca. 10 Hz, the appropriate NMR time scale can be approximated as (Ref. 61)

$$t_{\rm NMR} = (\sqrt{2}\pi |J|)^{-1} \approx 20 \text{ ms}. \qquad (11)$$

As the lifetime of Xe_2 in gas is eight orders of magnitude smaller than this estimate, the fast exchange process renders the J-coupling in the gas phase unobservable. Using the ACF depicted in the supplementary material,[41] we estimate the lifetime of Xe dimers in the present liquid simulation to be 40 ps, which is a somewhat smaller value than in the gas phase, most likely due to the more rapid dimer formation and reformation. This means that the coupling remains unobservable also in bulk liquid. Moreover, as opposed to the case of bulk xenon gas, no clear division into transient and persistent dimers can be detected. A low-temperature solid-state experiment on Xe would be interesting. In this case the chemical exchange rate is very slow, and the relevant dynamical processes are characterized by the T_1 relaxation time of ^{131}Xe, ca. 200 ms or more, depending on the temperature.[62]

It is noteworthy that via hyperpolarization of one of the coupled species the limitations of standard NMR due to exchange and diffusion mechanisms may be overcome, and a *sum* of the couplings from neighboring species [within the spatial range of the $J(r)$ function] may become observable via the frequency shifts that they cause.[15,63]

E. Xe dimer confined in cavities

The fact that the spatial range of the J-coupling interactions is limited, renders traditional NMR observation of $J(^{129}\mathrm{Xe} - {}^{131}\mathrm{Xe})$ difficult in bulk liquid or gas xenon. An

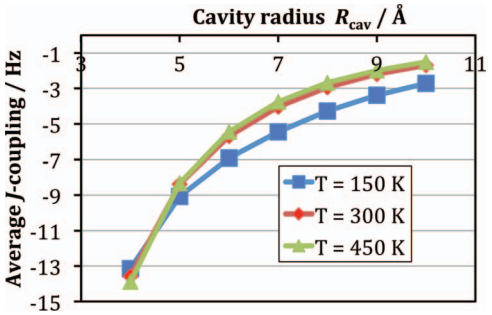

FIG. 4. Calculated average spin-spin coupling $\langle J(^{129}\mathrm{Xe} - {}^{131}\mathrm{Xe})\rangle$ in a xenon dimer confined to a simple spherical cavity model, as a function of the cavity radius $R_{\rm cav}$. The "Corr.+Rel." parametrization [Eq. (7)] of the spin-spin coupling curve $J(r)$ is used to calculate the average coupling according to Eq. (5), at three different temperatures.

TABLE III. Calculated average spin-spin coupling $\langle J(^{129}\mathrm{Xe} - {}^{131}\mathrm{Xe})\rangle$ (in Hz) in a xenon dimer confined to a simple spherical cavity model, as a function of the cavity radius R_{cav}. See Fig. 4 for details.

R_{cav} (Å)	$T = 150$ K	$T = 300$ K	$T = 450$ K
4	− 13.14	− 13.58	− 13.89
5	− 9.06	− 8.39	− 8.33
6	− 6.91	− 5.69	− 5.45
7	− 5.45	− 4.03	− 3.75
8	− 4.27	− 2.93	− 2.68
9	− 3.39	− 2.19	− 1.98
10	− 2.71	− 1.68	− 1.50

appealing alternative for experimental detection may be to confine interacting Xe atoms into a strictly limited region in space. When the internuclear Xe–Xe distance is constrained due to a confinement potential, the value of the average coupling may be expected to increase. Favorable conditions may occur for Xe_2 enclosed in microporous solids, fullerenes, or (provided that the lifetime of the complex is sufficient) clathrates. Figure 4 and Table III present the results for Xe dimer in our present, simplistic cavity model. For these results we have used presumably the best of the present parametrizations of the $J(r)$ curve, based on Eq. (7).

The results indicate that, indeed, couplings of the experimentally relevant magnitude are obtained in cavities with radii in the depicted range. The realistic minimum radius of a cavity that is capable of enclosing two xenon atoms is slightly less than 5 Å, due to the r_e separation of Xe nuclei in a free xenon dimer being ca. 4.4 Å. Neglecting the influence of the cavity wall on J(XeXe) renders the corresponding, maximum (absolute) value of the coupling to be roughly 10 Hz according to the "Corr.+Rel" parametrization, irrespective of the temperature in the range of 150–450 K. Couplings larger than 1.5 Hz in absolute value are still obtained for cavities with $R_{\mathrm{cav}} = 10$ Å, and for such larger cavities the low-temperature results ($T = 150$ K) are consistently larger than for the two higher temperatures, reflecting the fact that the thermal expansion of the Xe dimer plays a role in the larger cavities.

IV. CONCLUSIONS

We have carried out a relativistic quantum-chemical investigation of the indirect NMR spin-spin coupling in the prototypic van der Waals-bonded system, the Xe dimer. The spin-spin coupling constant as a function of the internuclear separation has been obtained nonrelativistically using different levels of theory, including an *ab initio* electron-correlated method, relativistically at the Hartree-Fock and DFT levels, as well as by hybrid approaches combining relativistic and electron correlation methods. The results indicate significant influence of relativistic effects on the monotonically decaying, negative $J(^{129}\mathrm{Xe} - {}^{131}\mathrm{Xe})$, cross-coupling between relativity and electron correlation, and experimentally relevant magnitude of the property (ca. −15 to − 13 Hz) at the equilibrium internuclear distance. Many-atom effects on $J(^{129}\mathrm{Xe} - {}^{131}\mathrm{Xe})$ are fairly small, but indicate a systematic trend upon increasing the coordination number of the Xe atoms. Simulated lifetime of Xe dimers in gaseous and liquid xenon is, however, tiny, as implied earlier, rendering these states unattractive for experimental observation of the average coupling $\langle J\rangle$, at least by normal thermally polarized, high-field techniques. When confining a xenon dimer into a material cavity of decreasing characteristic radius, the region of long internuclear separations and small $J(^{129}\mathrm{Xe} - {}^{131}\mathrm{Xe})$ are sampled to lesser extent, which makes the average coupling experimentally interesting, of the order of −10 Hz.

ACKNOWLEDGMENTS

Discussions with Dr. Ville-Veikko Telkki and Dr. Perttu Lantto, as well as Mr. Jarkko Vähäkangas (University of Oulu) are gratefully acknowledged. Financial support was received from the Academy of Finland, Tauno Tönning Fund, and University of Oulu. Computations were partially carried out at CSC - IT Center for Science Ltd. (Espoo, Finland).

[1] J. Vaara, J. Jokisaari, R. E. Wasylishen, and D. L. Bryce, Prog. Nucl. Magn. Reson. Spectrosc. **41**, 233 (2002); T. Helgaker, M. Jaszuński, and M. Pecul, *ibid.* **53**, 249 (2008).
[2] M. H. Levitt, *Spin Dynamics: Basics of Nuclear Magnetic Resonance*, 2nd ed. (Wiley, Chichester, 2007).
[3] M. Karplus, J. Chem. Phys. **30**, 11 (1959).
[4] P. R. Blake, J. B. Park, M. W. W. Adams, and M. F. Summers, J. Am. Chem. Soc. **114**, 4931 (1992); A. Dingley and S. Grzesiek, J. Am. Chem. Soc. **120**, 8293 (1998); K. Pervushin, A. Ono, C. Fernandez, T. Szyperski, M. Kainosho, and K. Wüthrich, Proc. Natl. Acad. Sci. U.S.A. **95**, 14147 (1998); I. G. Shenderovich, S. N. Smirnov, G. S. Denisov, V. A. Gindin, N. S. Golubev, A. Dunger, R. Reibke, S. Kirpekar, O. L. Malkina, and H.-H. Limbach, Ber. Bunsenges. Phys. Chem. **102**, 422 (1998).
[5] S. Grzesiek, F. Cordier, V. Jaravine, and M. Barfield, Prog. Nucl. Magn. Reson. Spectrosc. **45**, 275 (2004).
[6] A. Bagno, G. Saielli, and G. Scorrano, Angew. Chem., Int. Ed. **40**, 2532 (2001).
[7] A. Bagno, G. Saielli, and G. Scorrano, Chem.-Eur. J. **8**, 2047 (2002).
[8] F. R. Salsbury, Jr. and R. A. Harris, Mol. Phys. **94**, 307 (1998).
[9] A. Bagno and G. Saielli, Chem.-Eur. J. **9**, 1486 (2003).
[10] J. Autschbach and T. Ziegler, J. Chem. Phys. **113**, 936 (2000); **113**, 9410 (2000).
[11] M. Pecul, J. Chem. Phys. **113**, 10835 (2000).
[12] M. Pecul, J. Sadlej, and J. Leszczynski, J. Chem. Phys. **115**, 5498 (2001).
[13] H. Cybulski, M. Pecul, J. Sadlej, and T. Helgaker, J. Chem. Phys. **119**, 5094 (2003).
[14] A. Pikulska, M. Kauch, and M. Pecul, J. Phys. Chem. A **115**, 10795 (2011).
[15] M. P. Ledbetter, G. Saielli, A. Bagno, N. Tran, and M. V. Romalis, Proc. Natl. Acad. Sci. U.S.A. **109**, 12393 (2012).
[16] R. Bast, H. J. Aa. Jensen, T. Saue, L. Visscher *et al.*, DIRAC, a relativistic *ab initio* electronic structure program, Release DIRAC11, 2011 (see http://dirac.chem.vu.nl).
[17] L. Visscher, T. Enevoldsen, T. Saue, H. J. Aa. Jensen, and J. Oddershede, J. Comput. Chem. **20**, 1262 (1999); T. Enevoldsen, L. Visscher, T. Saue, H. J. Aa. Jensen, and J. Oddershede, J. Chem. Phys. **112**, 3493 (2000).
[18] J. Jokisaari, Prog. Nucl. Magn. Reson. Spectrosc. **26**, 1 (1994); D. Raftery, Annu. Rep. NMR Spectrosc. **57**, 205 (2006); P. Berthault, G. Huber, and H. Desvaux, Prog. Nucl. Magn. Reson. Spectrosc. **55**, 35 (2009).
[19] D. Raftery, H. Long, T. Meersmann, P. J. Grandinetti, L. Reven, and A. Pines, Phys. Rev. Lett. **66**, 584 (1991); T. G. Walker and W. Happer, Rev. Mod. Phys. **69**, 629 (1997).
[20] P. Pyykkö, E. Pajanne, and M. Inokuti, Int. J. Quantum Chem. **7**, 785 (1973).
[21] M. Hanni, P. Lantto, N. Runeberg, J. Jokisaari, and J. Vaara, J. Chem. Phys. **121**, 5908 (2004).
[22] M. Hanni, P. Lantto, M. Iliaš, H. J. Aa. Jensen, and J. Vaara, J. Chem. Phys. **127**, 164313 (2007).
[23] M. Straka, P. Lantto, M. Räsänen, and J. Vaara, J. Chem. Phys. **127**, 234314 (2007); P. Lantto, S. Standara, S. Riedel, J. Vaara, and M. Straka, Phys. Chem. Chem. Phys. **14**, 10944 (2012).

[24]P. Lantto, S. Kangasvieri, and J. Vaara, J. Chem. Phys. **137**, 214309 (2012).
[25]J.-H. Kantola, J. Vaara, T. T. Rantala, and J. Jokisaari, J. Chem. Phys. **107**, 6470 (1997).
[26]S. Komorovský, M. Repiský, O. L. Malkina, and V. G. Malkin, J. Chem. Phys. **132**, 154101 (2010).
[27]O. L. Malkina, S. Komorovský, L. Visscher, and V. G. Malkin, J. Chem. Phys. **134**, 086101 (2011).
[28]M. Hanni, P. Lantto, and J. Vaara, Phys. Chem. Chem. Phys. **13**, 13704 (2011).
[29]M. Hanni, P. Lantto, and J. Vaara, Phys. Chem. Chem. Phys. **11**, 2485 (2009).
[30]S. P. A. Sauer, J. Phys. B **30**, 3773 (1997).
[31]DALTON, a molecular electronic structure program, Release DALTON2011 (2011), see http://daltonprogram.org.
[32]M. Hanni, "Xe frequency shift in spin-exchange hyperpolarization mixture with Rb," unpublished work.
[33]P. Manninen and J. Vaara, J. Comput. Chem. **27**, 434 (2006).
[34]D. P. Chong, Can. J. Chem. **73**, 79 (1995).
[35]S. Ikäläinen, P. Lantto, P. Manninen, and J. Vaara, Phys. Chem. Chem. Phys. **11**, 11404 (2009); J. Vähäkangas, S. Ikäläinen, P. Lantto, and J. Vaara, "Nuclear magnetic resonance predictions for graphenes: concentric finite models and extrapolation to large systems," Phys. Chem. Chem. Phys. (in press).
[36]P. Lantto, K. Jackowski, W. Makulski, M. Olejniczak, and M. Jaszuński, J. Phys. Chem. A **115**, 10617 (2011).
[37]N. Abuzaid, A. M. Kantola, and J. Vaara, "Magnetic field-induced nuclear quadrupole coupling in atomic ^{131}Xe," Mol. Phys. (in press).
[38]S. Ikäläinen, P. Lantto, P. Manninen, and J. Vaara, J. Chem. Phys. **129**, 124102 (2008); S. Ikäläinen, M. V. Romalis, P. Lantto, and J. Vaara, Phys. Rev. Lett. **105**, 153001 (2010); T. S. Pennanen, S. Ikäläinen, P. Lantto, and J. Vaara, J. Chem. Phys. **136**, 184502 (2012); J. Shi, S. Ikäläinen, J. Vaara, and M. V. Romalis, J. Phys. Chem. Lett. **4**, 437 (2013); L.-j. Fu and J. Vaara, "Nuclear spin-induced Cotton-Mouton effect in molecules," J. Chem. Phys. (submitted).
[39]S. Ikäläinen, P. Lantto, and J. Vaara, J. Chem. Theory Comput. **8**, 91 (2012).
[40]J. Lehtola, P. Manninen, M. Hakala, and K. Hämäläinen, J. Chem. Phys. **137**, 104105 (2012).
[41]See supplementary material at http://dx.doi.org/10.1063/1.4793745 for tables of basis-set exponents, quantum-chemical data for the spin-spin coupling constant $J(^{129}\mathrm{Xe} - {}^{131}\mathrm{Xe})$ as a function of internuclear distance in xenon dimer, fitting parameters of the internuclear distance dependence, and illustration of the time autocorrelation function of the function indicating the existence of a Xe dimer.
[42]R. A. Aziz and M. J. Slaman, Mol. Phys. **57**, 825 (1986).
[43]M. Pecul, T. Saue, K. Ruud, and A. Rizzo, J. Chem. Phys. **121**, 3051 (2004).
[44]A. F. Maldonado and G. A. Aucar, Phys. Chem. Chem. Phys. **11**, 5615 (2009).
[45]J. Roukala, A. F. Maldonado, J. Vaara, G. A. Aucar, and P. Lantto, Phys. Chem. Chem. Phys. **13**, 21016 (2011).
[46]M. Olejniczak, R. Bast, T. Saue, and M. Pecul, J. Chem. Phys. **136**, 014108 (2012).
[47]L. Visscher, Theor. Chem. Acc. **98**, 68 (1997).
[48]R. Bast, T. Saue, J. Henriksson, and P. Norman, J. Chem. Phys. **130**, 024109 (2009).
[49]A. D. Becke, Phys. Rev. A **38**, 3098 (1988).
[50]C. Lee, W. Yang, and R. G. Parr, Phys. Rev. B **37**, 785 (1988).
[51]A. D. Becke, J. Chem. Phys. **98**, 5648 (1993); P. J. Stephens, F. J. Devlin, C. F. Chabalowski, and M. J. Frisch, J. Phys. Chem. **98**, 11623 (1994).
[52]A. D. Becke, J. Chem. Phys. **98**, 1372 (1993).
[53]P. Lantto and J. Vaara, J. Chem. Phys. **127**, 084312 (2007); M. Straka, P. Lantto, and J. Vaara, J. Phys. Chem. A **112**, 2658 (2008).
[54]B. Hess, C. Kutzner, D. van der Spoel, and E. Lindahl, J. Chem. Theory Comput. **4**, 435 (2008).
[55]A. Oros and N. J. Shah, Phys. Med. Biol. **49**, R105 (2004).
[56]S. Tsintsarska and H. Huber, Mol. Phys. **105**, 25 (2007).
[57]MATHEMATICA 8 (Wolfram Research Inc., 2011).
[58]J. Vaara, Phys. Chem. Chem. Phys. **9**, 5399 (2007).
[59]A. A. Auer and J. Gauss, Chem. Phys. **356**, 7 (2009).
[60]M. P. Allen and D. J. Tildesley, *Computer Simulation of Liquids* (Oxford University Press, 1987).
[61]R. G. Bryant, J. Chem. Educ. **60**, 933 (1983).
[62]W. W. Warren and R. E. Norberg, Phys. Rev. **148**, 402 (1966); **154**, 277 (1967).
[63]J. J. Heckman, M. P. Ledbetter, and M. V. Romalis, Phys. Rev. Lett. **91**, 067601 (2003).